Structural landscape of new salts of anti-histamine drug bilastine: Implications in physicochemical properties and anti-cancer activity against skin cancer

Manimurugan Kanagavel[a,c], Rajan Marystella Sparjan Samuvel[b,c], Vaikundamoorthy Ramalingam[b,c*], Sunil Kumar Nechipadappu[a,c*]

[a] Centre for X-ray Crystallography, Department of Analytical & Structural Chemistry, CSIR-Indian Institute of Chemical Technology, Hyderabad, India – 500 007.

[b] Department of Natural Products and Medicinal Chemistry, CSIR-Indian Institute of Chemical Technology, Hyderabad, India – 500 007.

[c] Academy of Scientific and Innovative Research (AcSIR), Ghaziabad, 201002, India

*Corresponding authors: *nsunilkumar@iict.res.in* and *ramalingam@iict.res.in*

Table of Contents

Table S1 Hydrogen-bond geometry of BLN salts (Å, º).

D—H···A	D—H	H···A	D···A	D—H···A
BLN^{+}-Cl^{-}-$3H_2O$				
O1W—H2W···Cl01^{i}	0.83 (3)	2.45 (3)	3.2700 (15)	175 (2)
O3W—H5W···Cl01^{i}	0.90 (3)	2.41 (3)	3.3016 (14)	171 (2)
O2W—H3W···Cl01^{ii}	0.84 (3)	2.36 (3)	3.1851 (14)	167 (2)
O2W—H4W···N2^{ii}	0.88 (2)	2.02 (2)	2.8896 (17)	173 (2)
O3W—H6W···O2W	0.92 (3)	2.04 (3)	2.9616 (19)	172 (2)
N3—H3N···Cl01	0.944 (18)	2.139 (18)	3.0766 (13)	171.9 (15)
O3—H3O···O1W	0.85 (2)	1.81 (2)	2.6536 (17)	174 (2)
O1W—H1W···O2W	0.87 (3)	1.95 (3)	2.8215 (17)	172 (2)
Symmetry codes: (i) −x+3/2, y+1/2, −z+3/2; (ii) x−1/2, −y+1/2, z+1/2.				
BLN^{+}-Cl^{-}-$4H_2O$				
O3—H3O···N2^{i}	0.89 (5)	1.73 (5)	2.594 (3)	164 (4)
O1W—H1W···O2W	0.81 (2)	1.95 (3)	2.744 (4)	166 (4)
O1W—H2W···Cl1^{ii}	0.82 (2)	2.32 (3)	3.113 (3)	163 (4)
O2W—H3W···O3W	0.88 (2)	1.88 (3)	2.734 (4)	162 (4)
O2W—H4W···O4W	0.89 (2)	1.85 (3)	2.744 (4)	174 (4)
O3W—H5W···O2^{iii}	0.84 (2)	2.03 (3)	2.854 (3)	165 (4)
O3W—H6W···Cl1^{iv}	0.87 (3)	2.27 (3)	3.137 (3)	173 (5)
O4W—H7W···O1^{iv}	0.95 (6)	1.95 (6)	2.857 (4)	159 (5)
O4W—H8W···Cl1	0.79 (4)	2.33 (4)	3.117 (3)	175 (4)
N3—H3N···O1W	0.86 (4)	1.94 (4)	2.786 (3)	168 (4)
Symmetry codes: (i) *x*, *y*, *z*+1; (ii) *x*+1, *y*, *z*; (iii) −*x*+2, *y*+1/2, −*z*+2; (iv) −*x*+1, *y*+1/2, −*z*+1.				
BLN^{+}-Br^{-}-H_2O				
O3—H3O···O2^{i}	0.80 (2)	1.83 (2)	2.6271 (16)	177 (2)
O1W—H1W···N2	0.78 (3)	2.09 (3)	2.8707 (18)	177 (3)
O1W—H2W···Br1	0.77 (2)	2.60 (2)	3.3754 (13)	177 (2)
N3—H3N···Br1	0.89 (2)	2.37 (2)	3.2475 (12)	165.8 (17)
Symmetry code: (i) −x+1, −y, −z+1.				
BLN^{2+}-NO_3^{2-}-H_2O				
N3—H3N···O4^{i}	0.95 (3)	2.48 (3)	2.985 (3)	113 (2)
N2—H2N···N4	0.89 (2)	2.56 (2)	3.426 (4)	162 (3)
N2—H2N···O5	0.89 (2)	2.52 (3)	3.216 (4)	136 (3)
N2—H2N···O6	0.89 (2)	1.88 (2)	2.753 (4)	167 (3)
N3—H3N···O1W	0.95 (3)	1.92 (3)	2.823 (4)	157 (3)
O3—H3O···N5	0.84	2.48	3.321 (8)	176
O3—H3O···O7	0.84	2.35	3.111 (12)	152
O3—H3O···O8	0.84	1.80	2.544 (6)	147
O1W—H1W···O6	0.86 (1)	2.10 (3)	2.873 (5)	150 (6)
Symmetry code: (i) −x+1, −y+1, −z+1.				
BLN^{2+}-SO_4^{2-}-$4H_2O$				
O6—H6O···S1^{i}	0.84	2.72	3.510 (4)	157
O6—H6O···O5^{i}	0.84	1.74	2.570 (5)	168
O3W—H5W···S2^{iii}	0.86 (1)	3.00 (3)	3.783 (5)	152 (6)
O4W—H7W···O3^{iii}	0.86 (1)	1.99 (1)	2.842 (6)	173 (6)
O4W—H8W···O8^{iv}	0.86 (1)	2.06 (3)	2.823 (8)	148 (6)
O9—H9O···O3W	0.86 (1)	1.65 (1)	2.509 (7)	175 (8)
O1W—H1W···S2	0.86 (1)	2.90 (1)	3.758 (6)	175 (10)
O1W—H1W···O11	0.86 (1)	1.86 (5)	2.645 (17)	151 (10)
O1W—H2W···O2W	0.86 (1)	2.10 (10)	2.726 (10)	130 (11)
O3W—H6W···O4W	0.86 (1)	1.81 (1)	2.670 (6)	172 (6)

N2—H2···O5	0.88	1.90	2.780 (5)	173
N3—H3···S1	1.00	2.94	3.883 (4)	158
N3—H3···O4	1.00	1.83	2.779 (5)	157
O2—H2O···O1W	0.99 (7)	1.56 (7)	2.525 (7)	163 (6)
Symmetry codes: (i) x, −y+3/2, z−1/2; (ii) −x+1, −y+1, −z−2; (iii) −x, −y+1, −z−2; (iv) −x, −y+1, −z−3.				
BLN^+-$H_2PO_4^-$-2MeOH				
N3—H3N···O7^{i}	0.85 (5)	1.83 (5)	2.683 (4)	178 (5)
O2—H2O···O5	0.87 (7)	1.78 (8)	2.613 (4)	160 (7)
O4—H4O···O7^{ii}	0.83 (5)	1.74 (5)	2.554 (4)	169 (5)
O6—H6O···N2^{iii}	0.83 (6)	1.83 (6)	2.663 (4)	174 (5)
O8a—H8Oa···O5	0.84	2.04	2.776 (11)	145
O9-H9O···O8	0.84	2.08	2.794 (16)	142
Symmetry codes: (i) −x+2, −y+1, −z+1; (ii) −x+2, −y+1, −z; (iii) x, y, z−1.				
BLN^+-$H_2PO_4^-$-Cl^--3H_2O				
O1W—H2W···Cl1^{i}	0.98 (2)	2.17 (2)	3.1378 (12)	172.6 (18)
O2W—H4W···O1B^{ii}	0.86 (2)	2.05 (2)	2.9073 (15)	172 (2)
N3B—H3NB···Cl1	0.900 (17)	2.276 (18)	3.1624 (12)	168.3 (14)
O2B—H2OB···O1	1.04 (5)	1.44 (5)	2.4793 (16)	172 (3)
O2B—H2OB···O3	1.04 (5)	2.65 (4)	3.2955 (14)	119 (2)
O1—H1O···O2B	0.64 (5)	1.84 (5)	2.4793 (16)	174 (6)
O1—H1O···O3B	0.64 (5)	2.86 (5)	3.3183 (16)	131 (5)
O1—H1O···O2B	0.64 (5)	1.84 (5)	2.4793 (16)	174 (6)
O3—H3O···O3B	0.93 (2)	1.64 (3)	2.5709 (15)	176 (2)
O4—H4O···O2A	0.85 (2)	1.80 (2)	2.647 (3)	176 (2)
O1W—H1W···O2W	0.84 (2)	1.90 (2)	2.7316 (16)	172 (2)
O2W—H3W···N2A	0.91 (2)	1.99 (2)	2.8971 (16)	175 (2)
O3W—H5W···N2B	0.94 (2)	1.95 (2)	2.8562 (16)	162 (2)
O3W—H6W···Cl1	0.92 (2)	2.32 (2)	3.2383 (14)	172.3 (19)
N3A—H3NA···O1W	0.906 (17)	1.821 (18)	2.7253 (16)	176.2 (15)
O3A—H3OA···O2	0.99 (2)	1.49 (3)	2.4697 (14)	173 (2)
Symmetry codes: (i) x, y−1, z−1; (ii) x−1, y−1, z−1.				

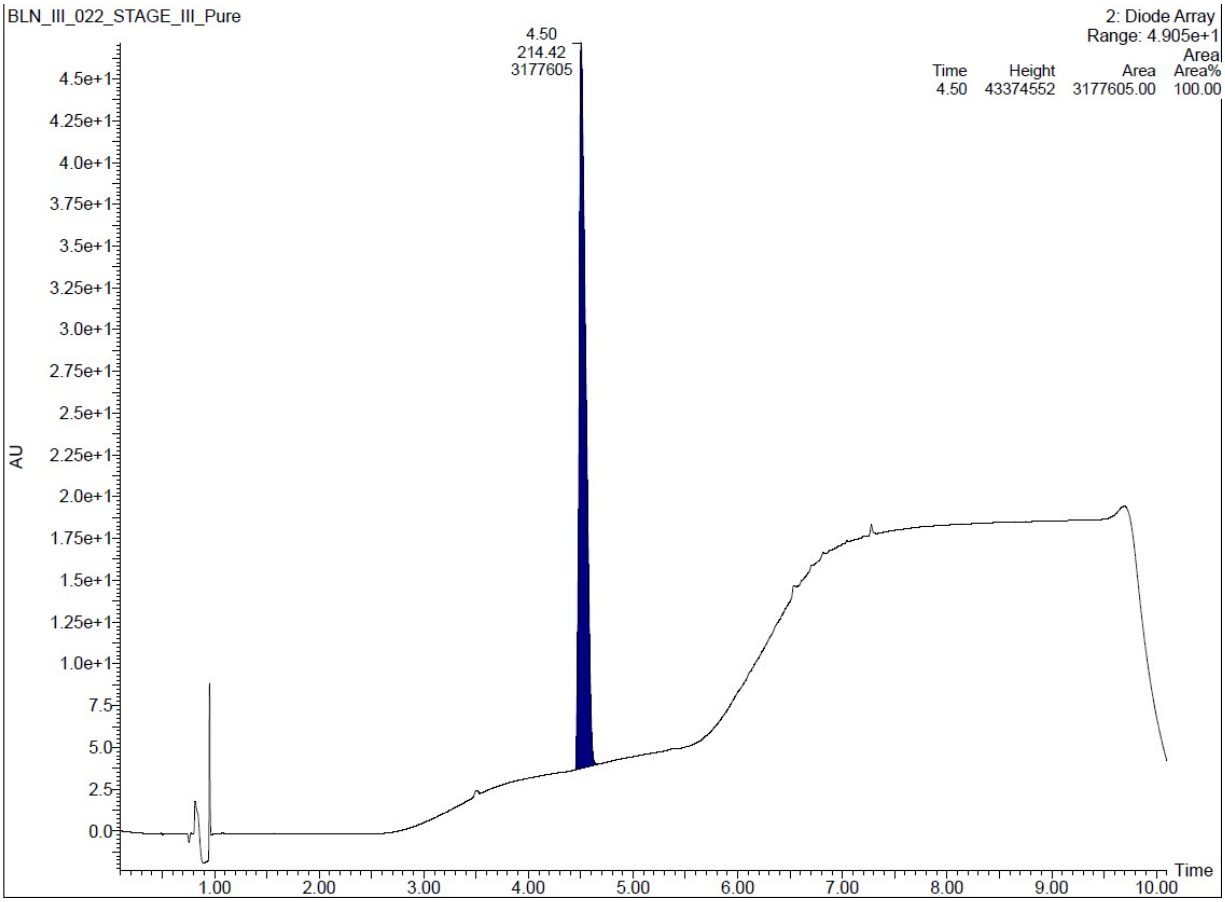

Fig. S1 UPLC chromatogram of BLN.

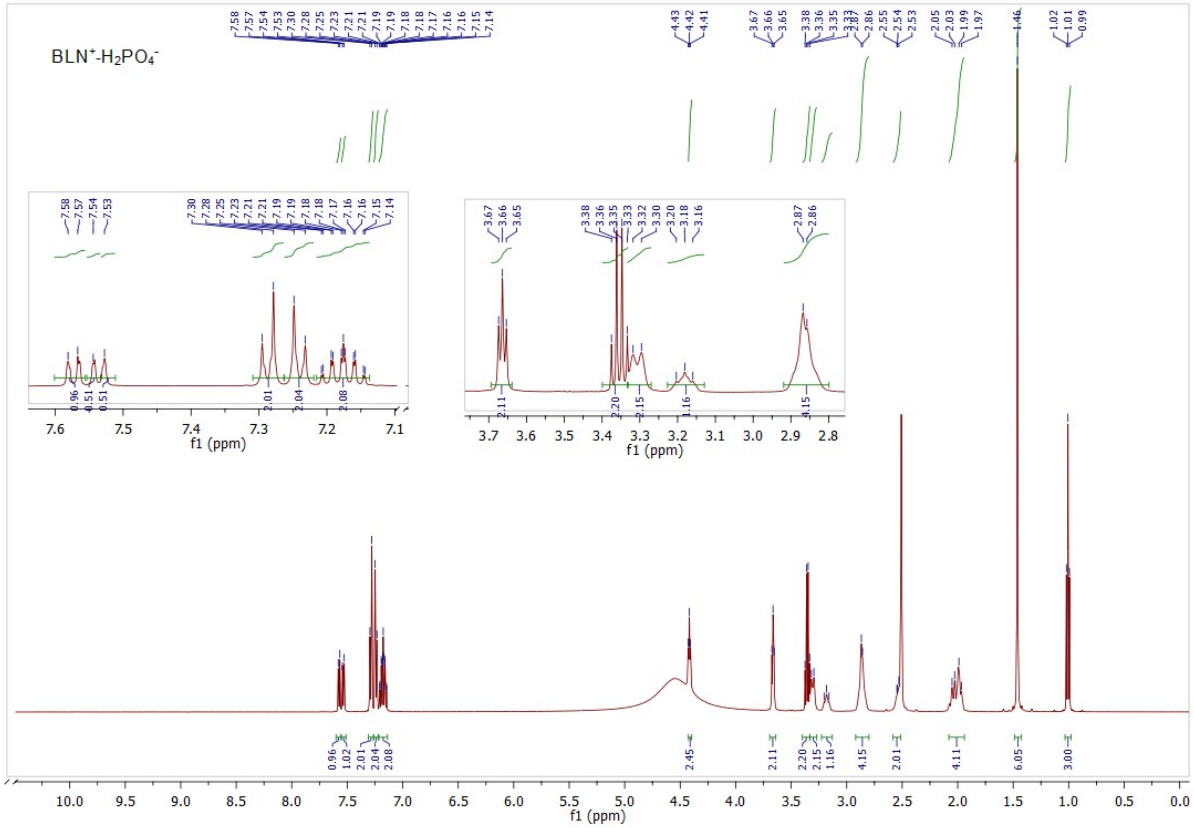

Fig. S2 ^{1}H NMR of BLN^{+}-$H_2PO_4^{-}$ (400 MHz, DMSO-d6) δ-ppm: 0.99- 1.02 (t, 3H), 1.46 (S, 6H), 1.97- 2.07 (m, 4H), 2.53- 2.55 (m, 2H), 2.86-2.87 (d, 4H), 3.16-3.20 (t, 1H), 3.30- 3.32 (m, 2H), 3.33-3.38 (q,2H), 3.65- 3.67 (t, 2H), 4.41-4.43 (t, 2H), 7.14-7.30 (m, 6H), 7.53-7.58 (m, 2H).

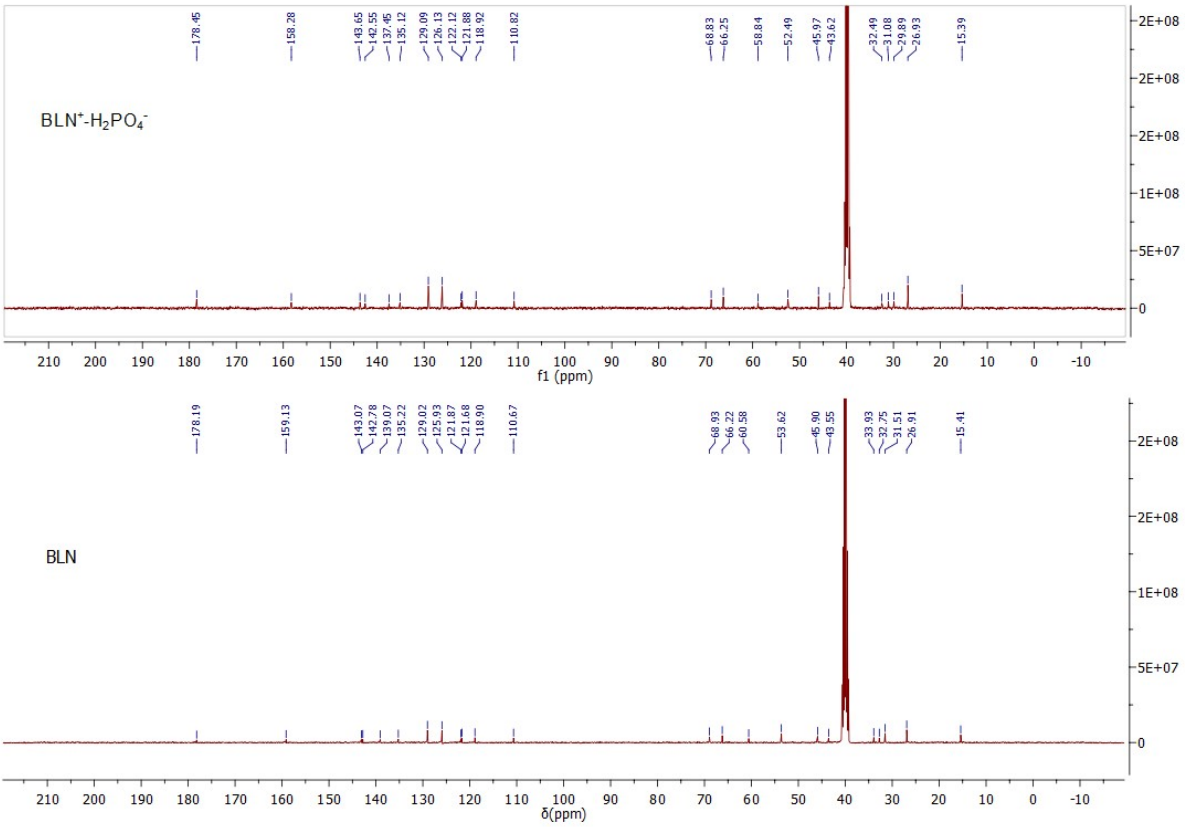

Fig. S3 ^{13}C NMR overlay of BLN and BLN^{+}-$H_2PO_4^{-}$ (100 MHz, DMSO-d6) δ-ppm

BLN^{+}-$H_2PO_4^{-}$: 15.39, 26.93, 31.08, 32.49, 43.62, 45.97, 52.49, 58.34, 66.25, 68.83, 110.82, 118.92, 121.88, 122.12, 126.13, 129.09, 135.12, 137.45,142.55, 142.55, 158.28, 178.48.

BLN: 15.41, 26.91, 31.51, 32.75, 33.93, 43.55, 45.90, 53.62, 60.58, 66.22, 68.93, 110.67, 118.90, 121.68, 121.87, 125.93, 129.02, 135.22, 139.07, 142.78, 143.07, 159.13, 178.19.

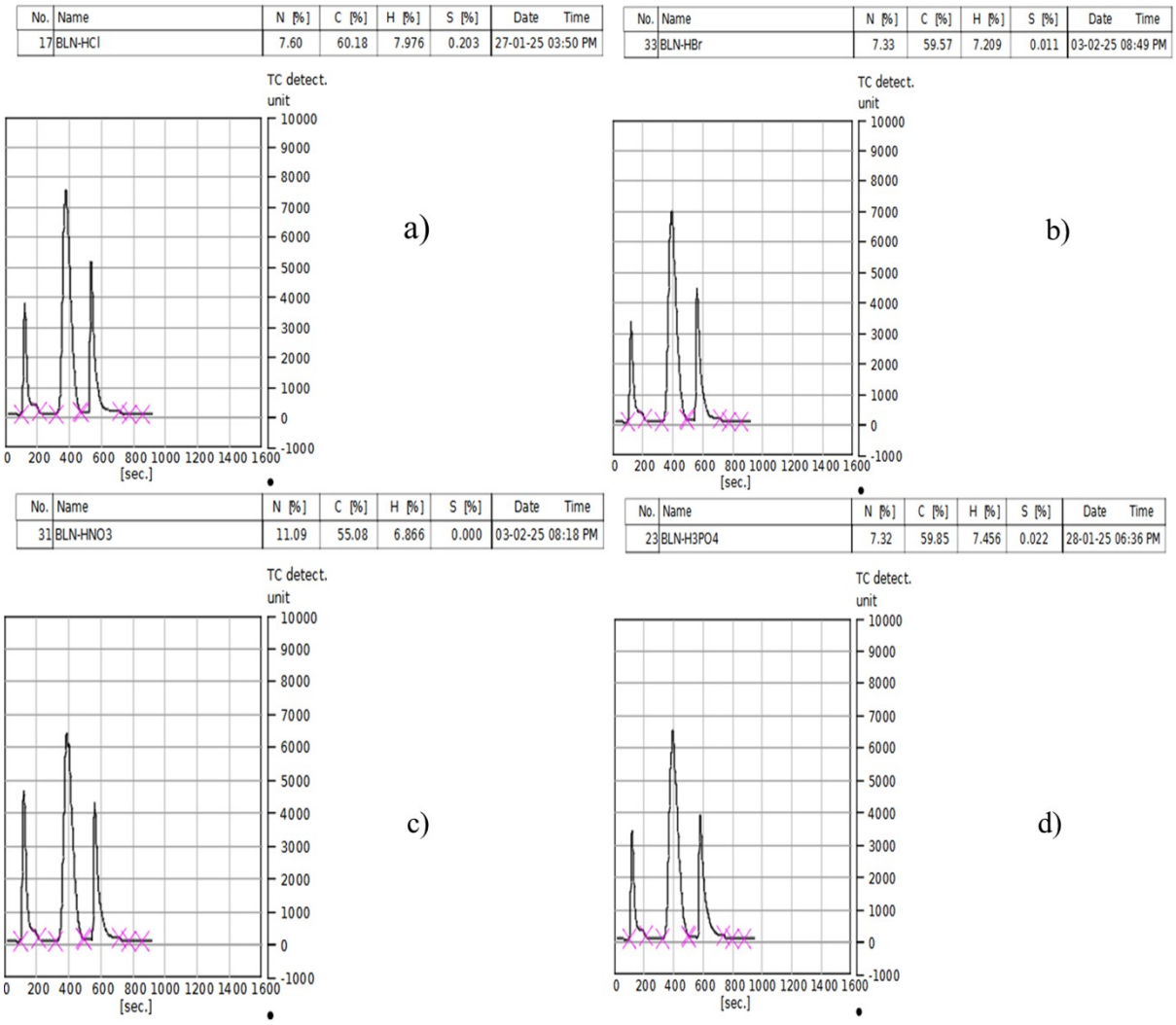

Fig. S4 CHN analysis plot of BLN salts a) BLN^{+}-Cl^{-}-$3H_2O$, b) BLN^{+}-Br^{-}-H_2O, c) BLN^{2+}-NO_3^{2-}-H_2O, and d) BLN^{+}-$H_2PO_4^{-}$.

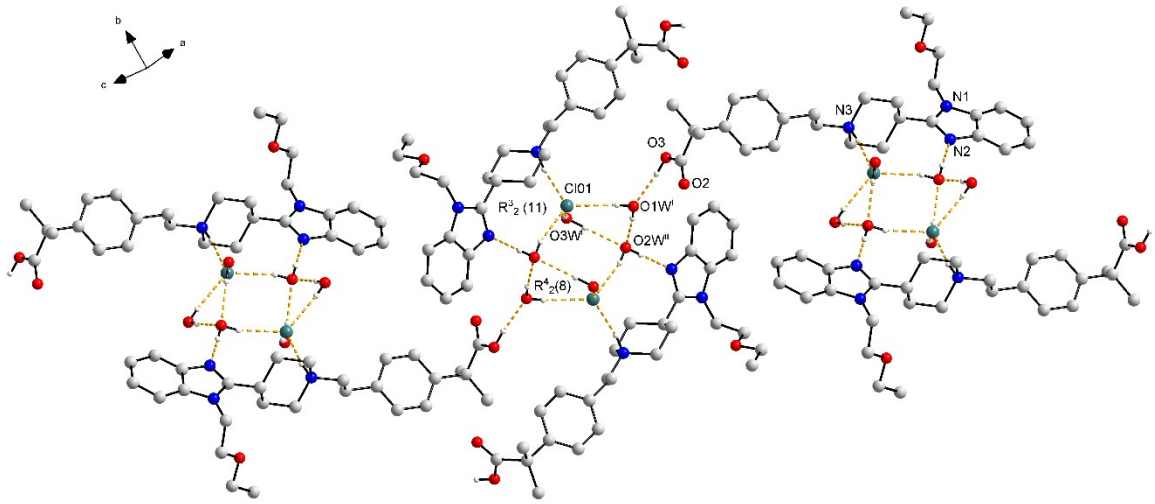

Fig. S5 The crystal packing of BLN^{+}-Cl^{-}-$3H_2O$ showing the symmetry codes of hydrogen bond interaction.

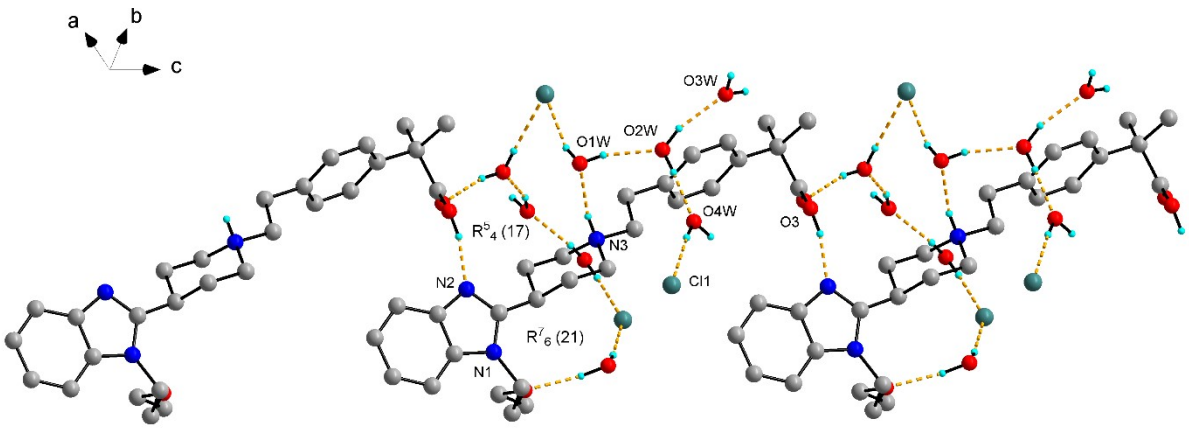

Fig. S6 The crystal packing diagram of BLN^+-Cl^--$4H_2O$ showing the hydrogen bond interactions and ring motifs.

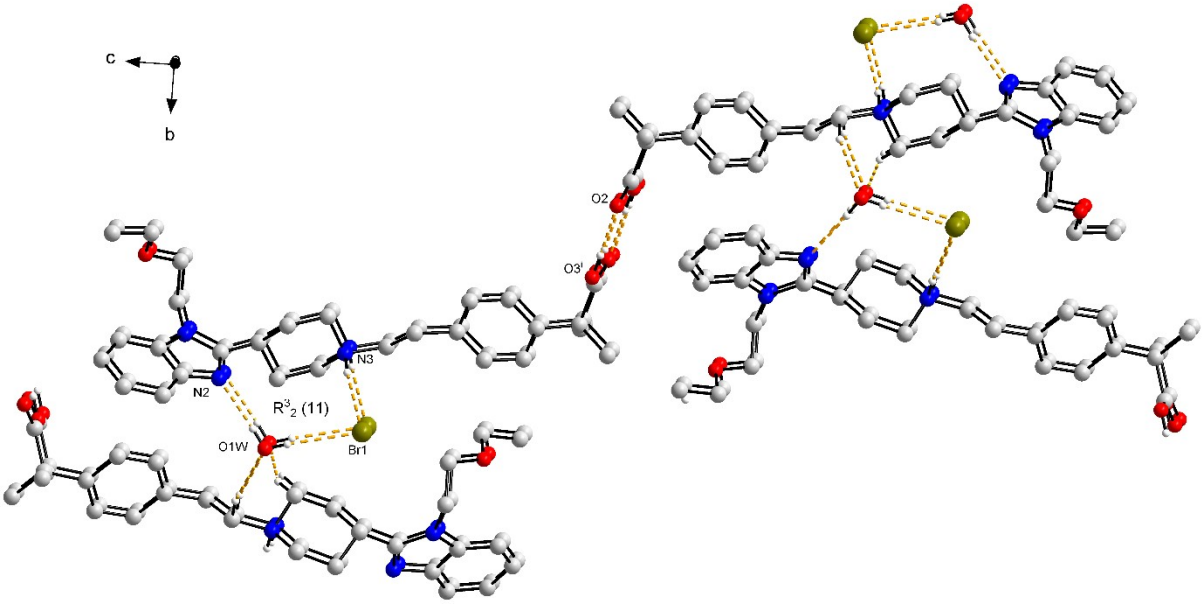

Fig. S7 The crystal packing diagram of BLN^+-Br^--H_2O showing the hydrogen bond interactions and ring motifs.

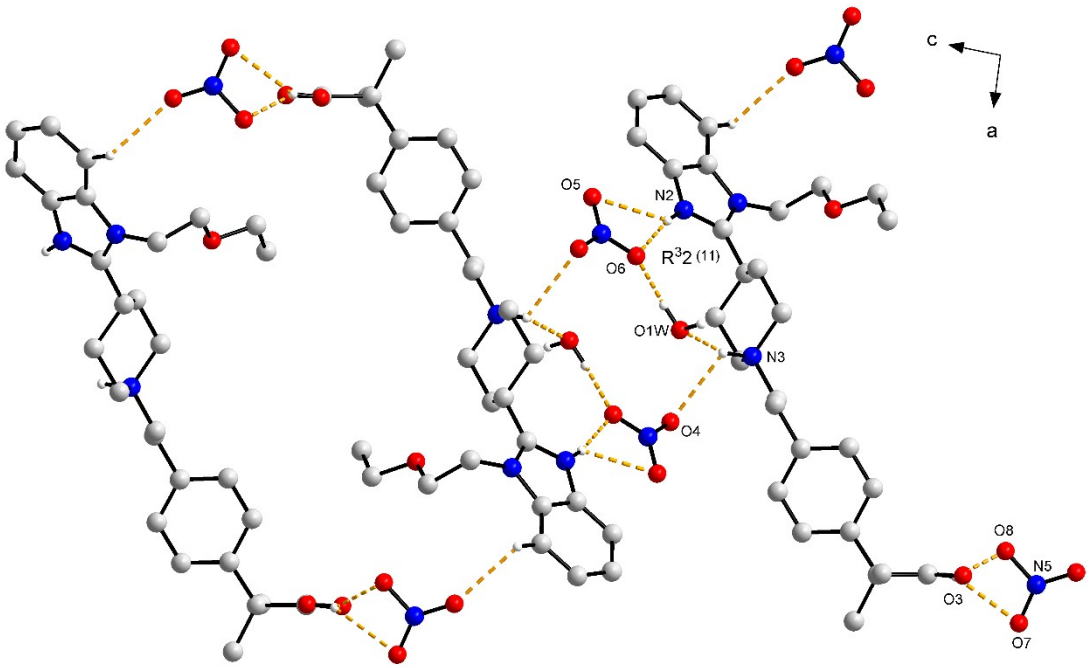

Fig. S8 The crystal packing diagram of BLN^{2+}-NO_3^{2-}-H_2O showing the hydrogen bond interactions and ring motifs.

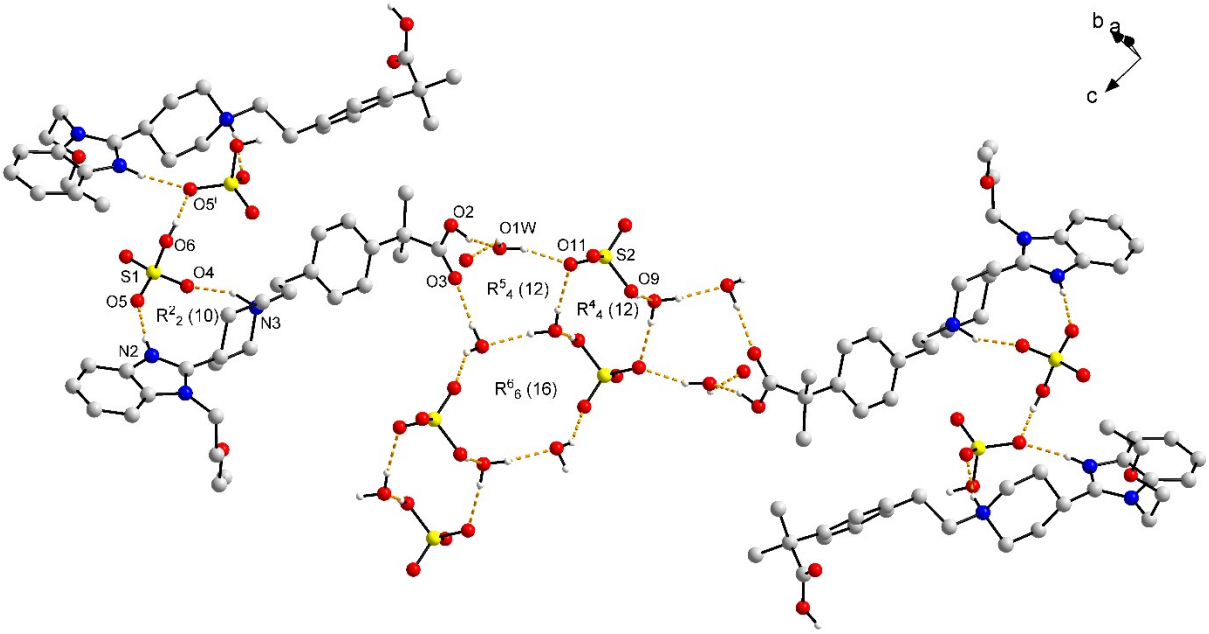

Fig. S9 The crystal packing diagram of BLN^{2+}-SO_4^{2-}-$4H_2O$ showing the hydrogen bond interactions and ring motifs.

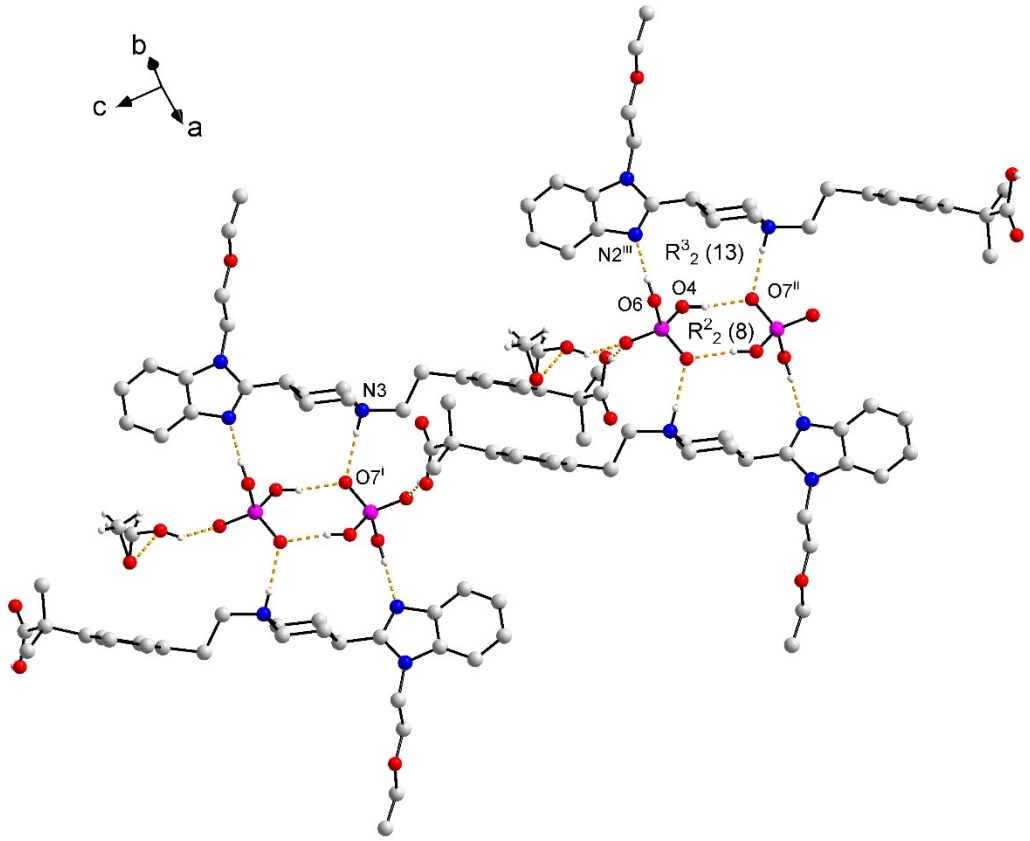

Fig. S10 The crystal packing diagram of BLN^{+}-$H_2PO_4^{-}$-2MeOH showing the hydrogen bond interactions and ring motifs.

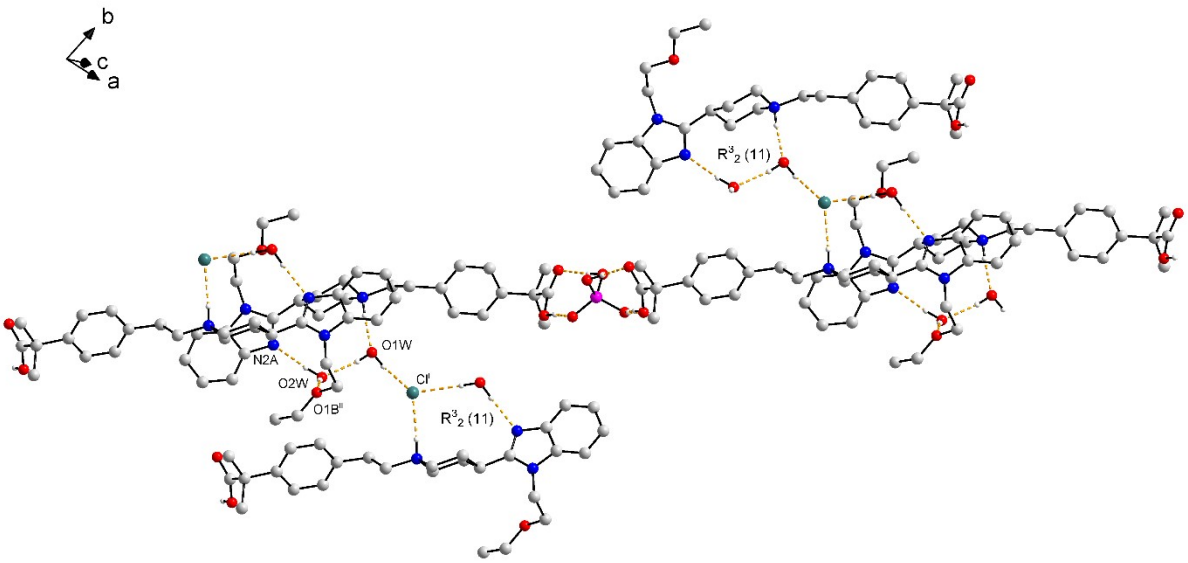

Fig. S11 The crystal packing diagram of BLN^{+}-$H_2PO_4^{-}$-Cl^{-}-$3H_2O$ showing the hydrogen bond interactions and ring motifs.

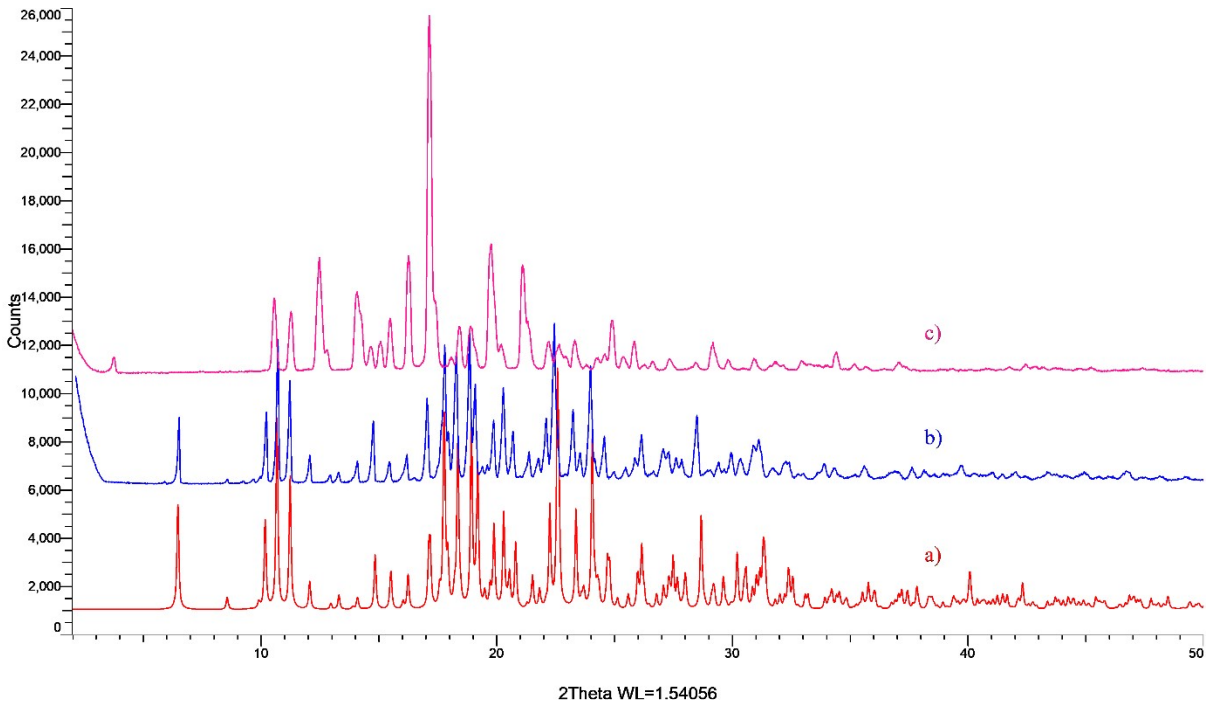

Fig. S12 PXRD powder pattern overlay of (a) BLN^{+}-Cl^{-}-$3H_2O$ simulated and (b) BLN^{+}-Cl^{-}-$3H_2O$ experimental with (c) BLN Form-I.

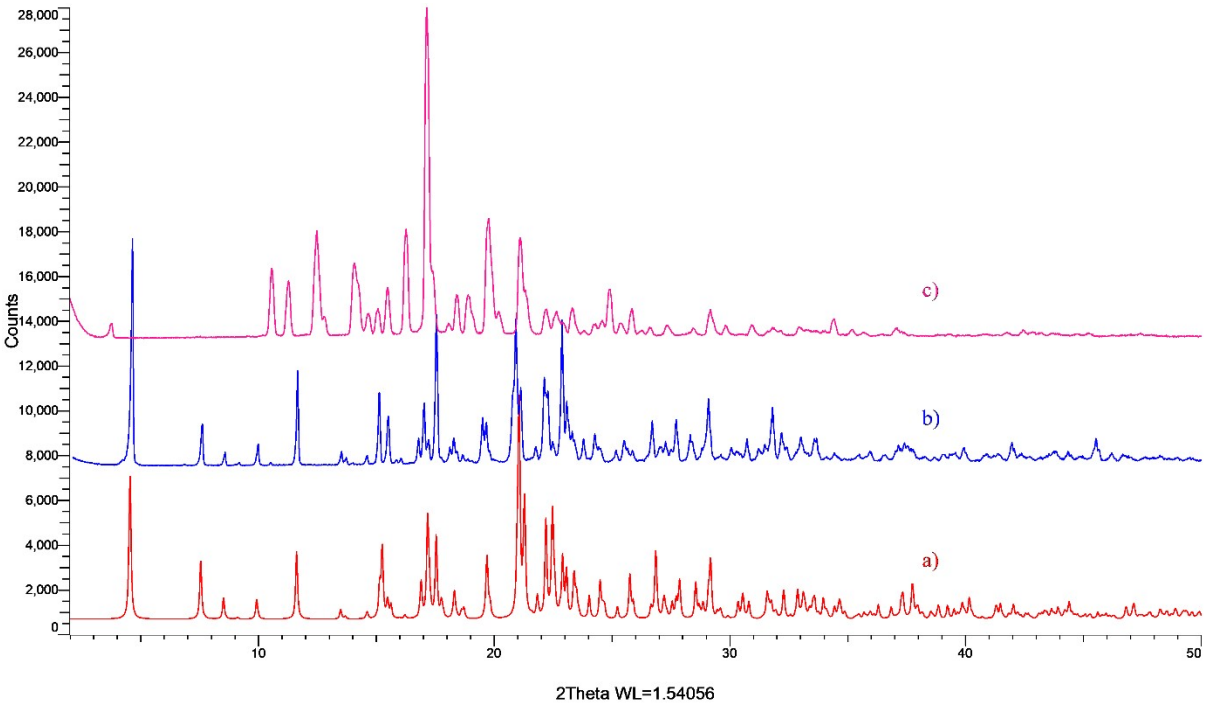

Fig. S13 PXRD powder pattern overlay of (a) BLN^{+}-Br^{-}-H_2O simulated and (b) BLN^{+}-Br^{-}-H_2O experimental with (c) BLN Form-I.

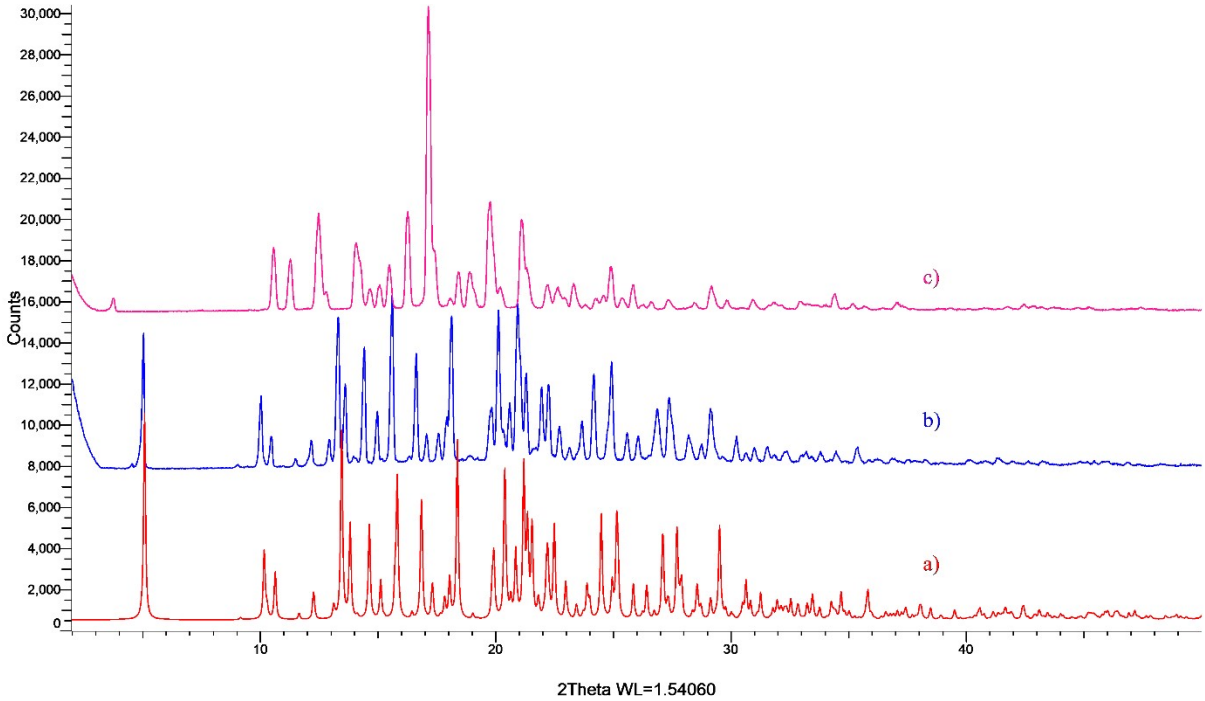

Fig. S14 PXRD powder pattern overlay of (a) BLN^{2+}-NO_3^{2-}-H_2O simulated and (b) BLN^{2+}-NO_3^{2-}-H_2O experimental with (c) BLN Form-I.

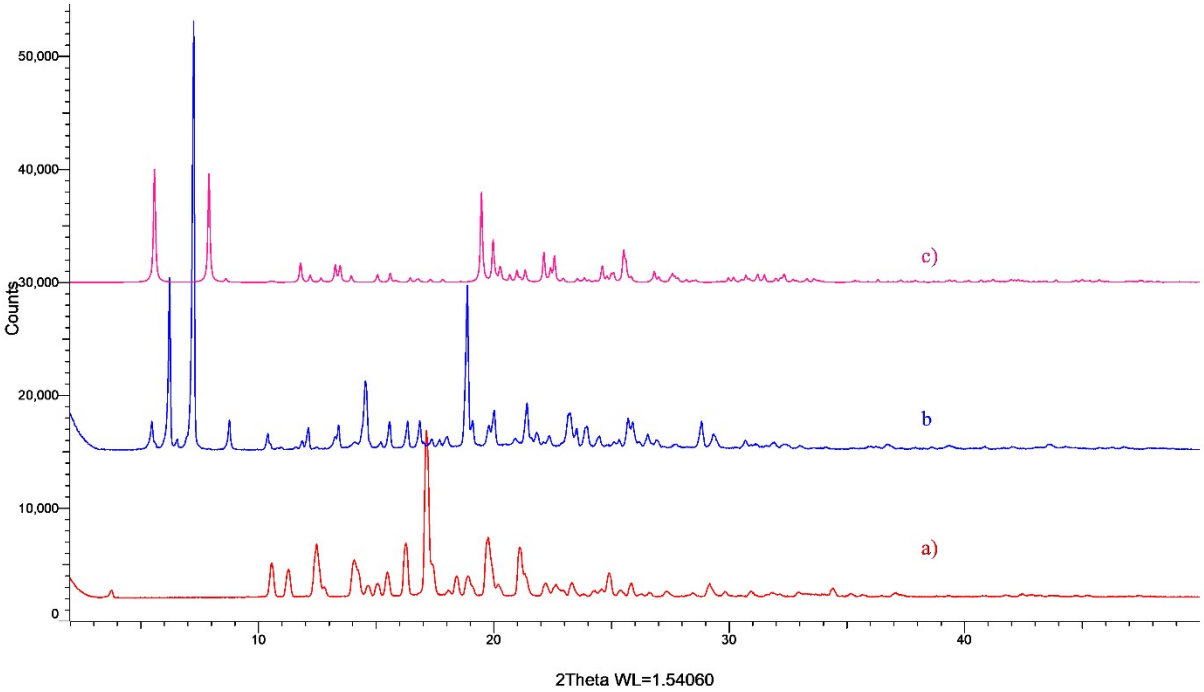

Fig. S15 PXRD powder pattern overlay of (a) BLN Form-I (b) BLN^{+}-$H_2PO_4^{-}$ experimental (c) BLN^{+}-$H_2PO_4^{-}$-2MeOH simulated.

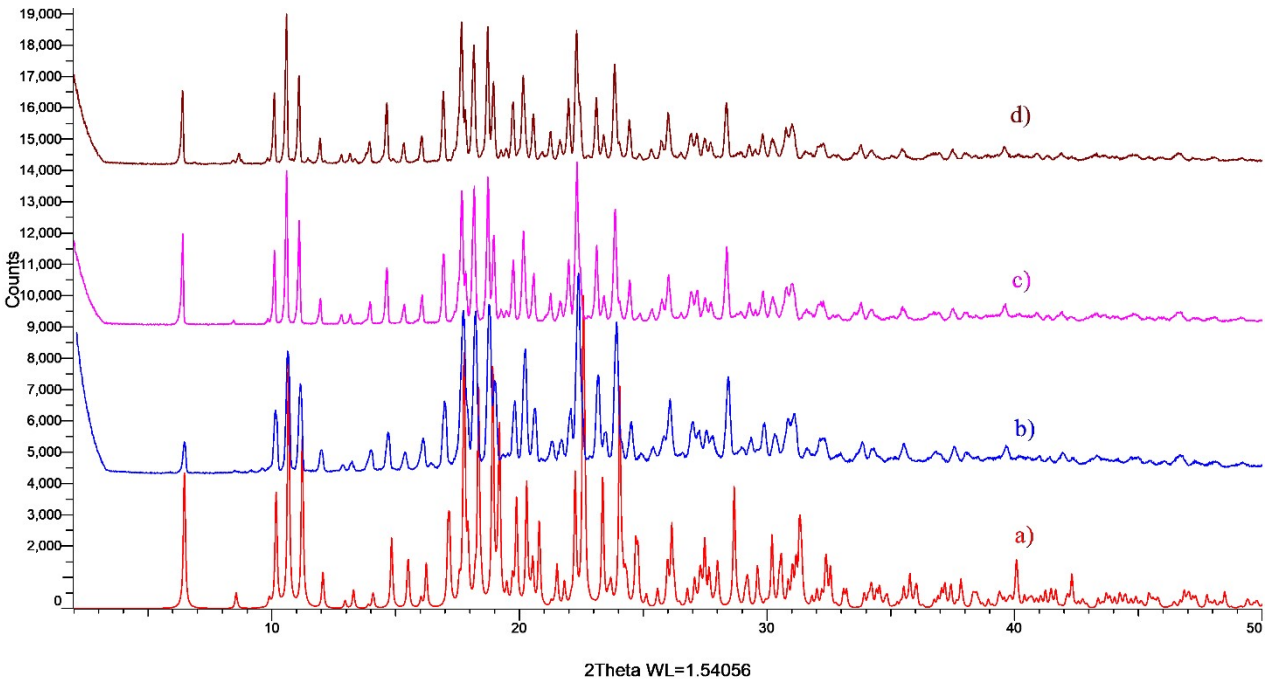

Fig. S16 PXRD powder pattern overlay of stability samples at room temperature (a) BLN^{+}-Cl^{-}-$3H_2O$ simulated (b) BLN^{+}-Cl^{-}-$3H_2O$ experimental after one month (c) BLN^{+}-Cl^{-}-$3H_2O$ experimental after two months d) BLN^{+}-Cl^{-}-$3H_2O$ experimental after three months.

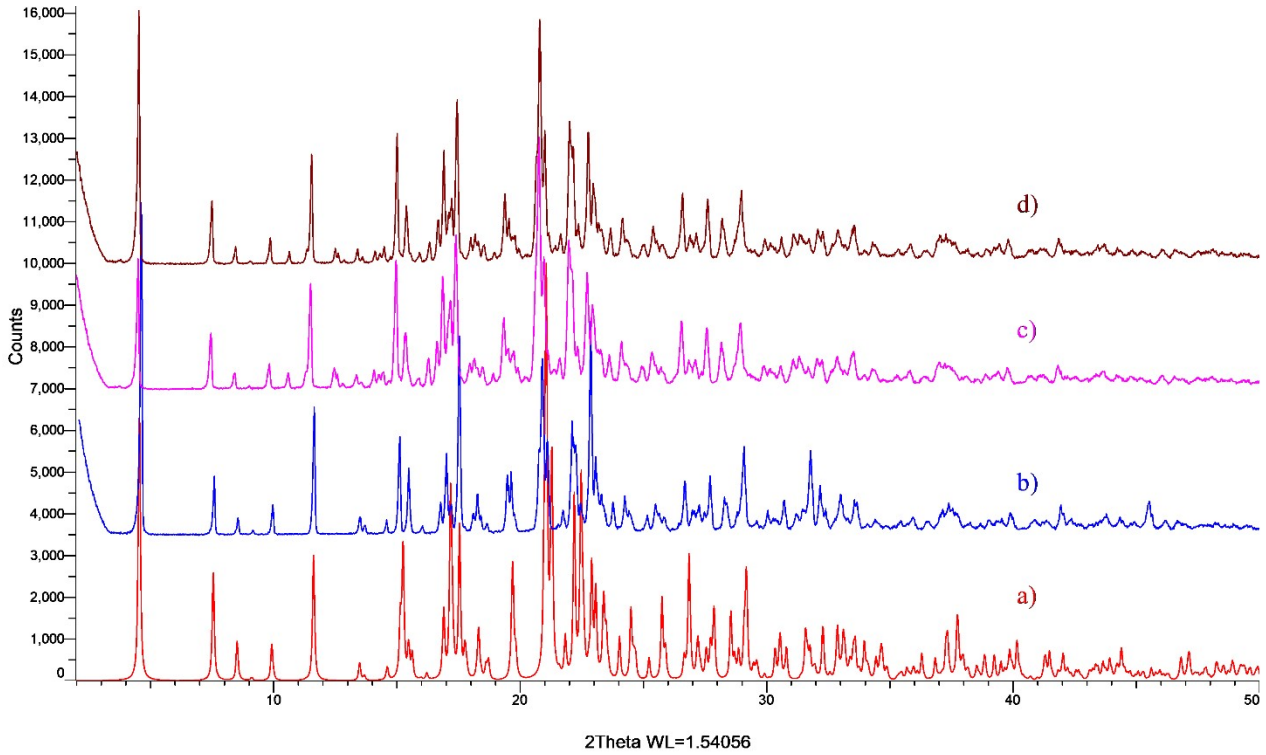

Fig. S17 PXRD powder pattern overlay of stability samples at room temperature (a) BLN^{+}-Br^{-}-H_2O simulated and (b) BLN^{+}-Br^{-}-H_2O experimental after one month (c) BLN^{+}-Br^{-}-H_2O experimental after two months d) BLN^{+}-Br^{-}-H_2O experimental after three months.

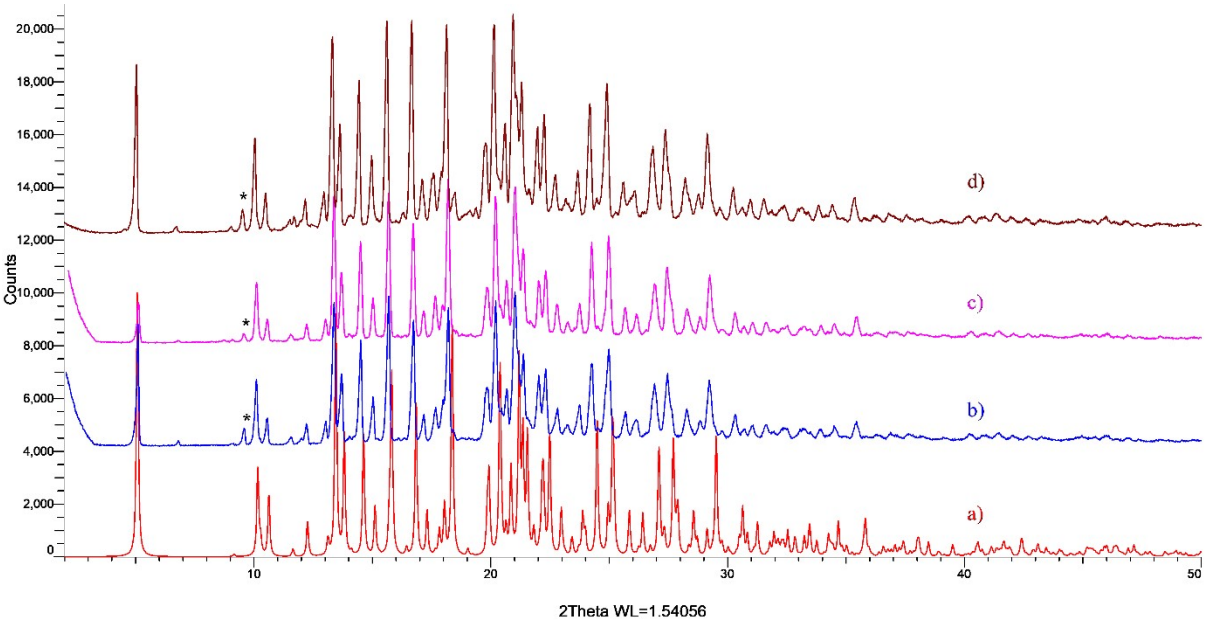

Fig. S18 PXRD powder pattern overlay of stability samples at room temperature (a) BLN^{2+}-NO_3^{2-}-H_2O simulated and (b) BLN^{2+}-NO_3^{2-}-H_2O experimental after one month (c) BLN^{2+}-NO_3^{2-}-H_2O experimental after two months d) BLN^{2+}-NO_3^{2-}-H_2O experimental after three months (* indicates the unaccounted peak).

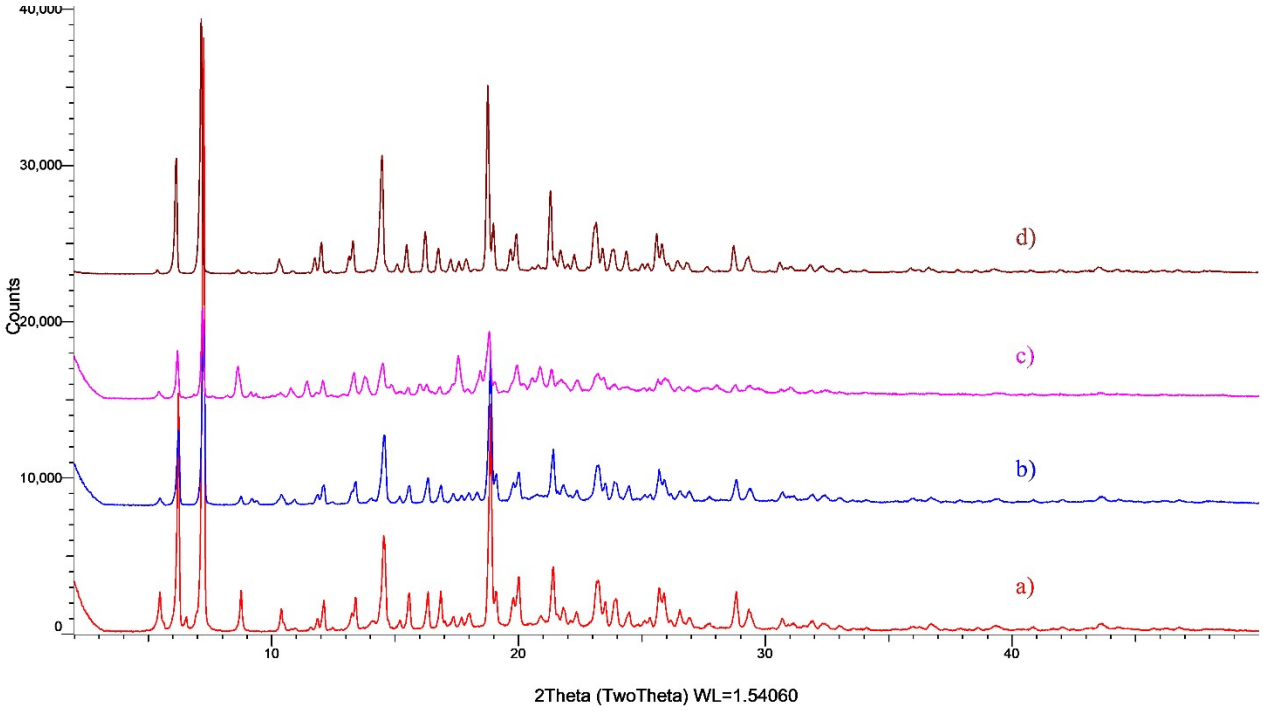

Fig. S19 PXRD powder pattern overlay of (a) BLN^{+}-$H_2PO_4^{-}$ experimental initial (b) BLN^{+}-$H_2PO_4^{-}$ experimental after one month (c) BLN^{+}-$H_2PO_4^{-}$ experimental after two months d) BLN^{+}-$H_2PO_4^{-}$ experimental after three months.

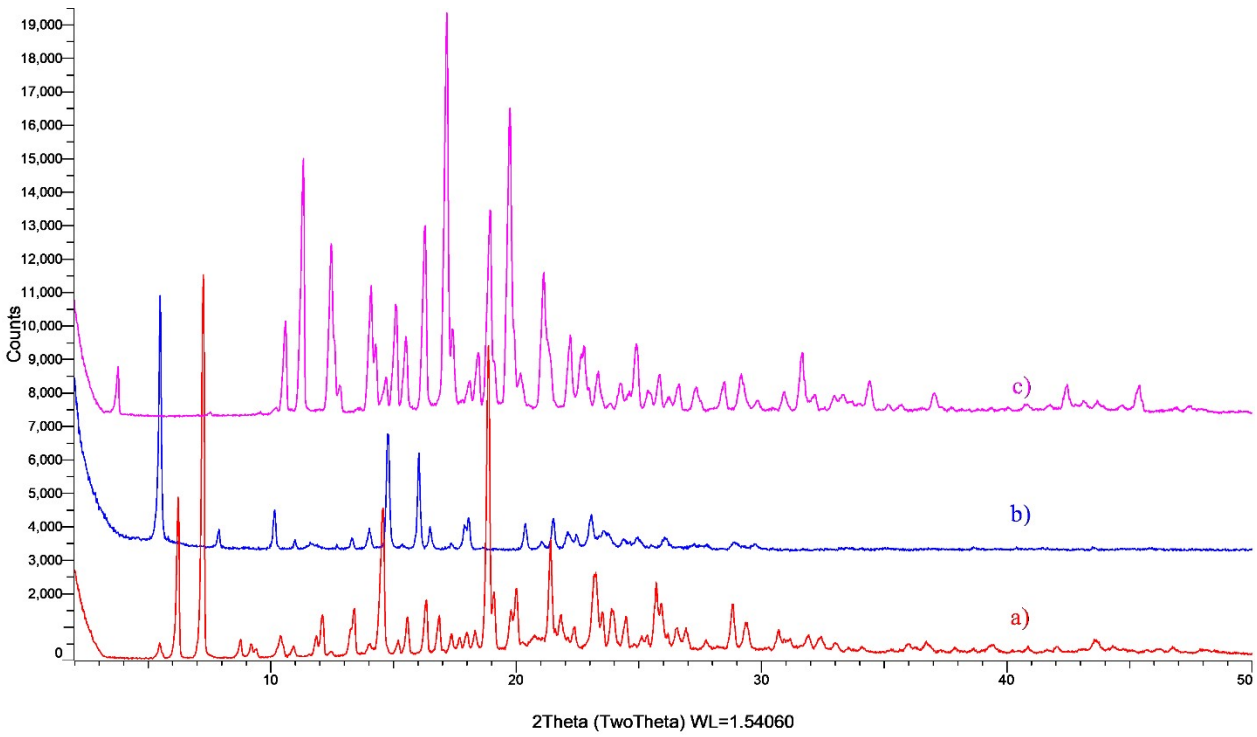

Fig. S20 PXRD powder pattern overlay of stability samples at room temperature (a) BLN^+-$H_2PO_4^-$ experimental and (b) BLN^+-$H_2PO_4^-$ after heating to first endotherm (200 °C) with (c) BLN Form-I.

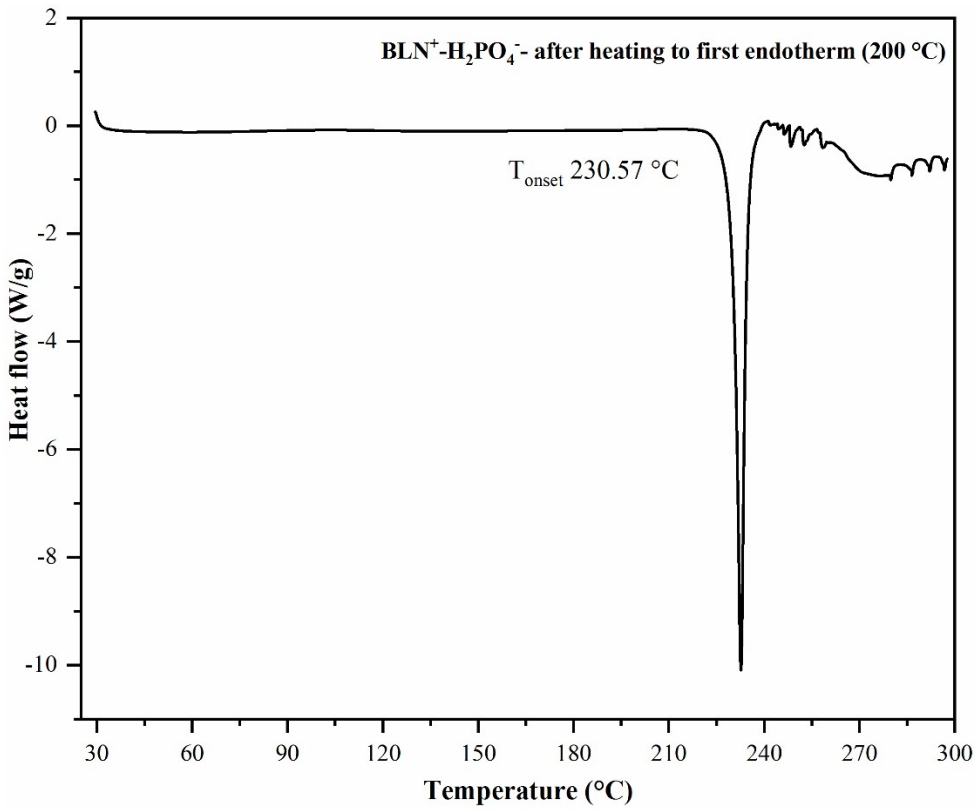

Fig. S21 DSC plot of BLN^+-$H_2PO_4^-$ preheated sample (up to first endotherm).

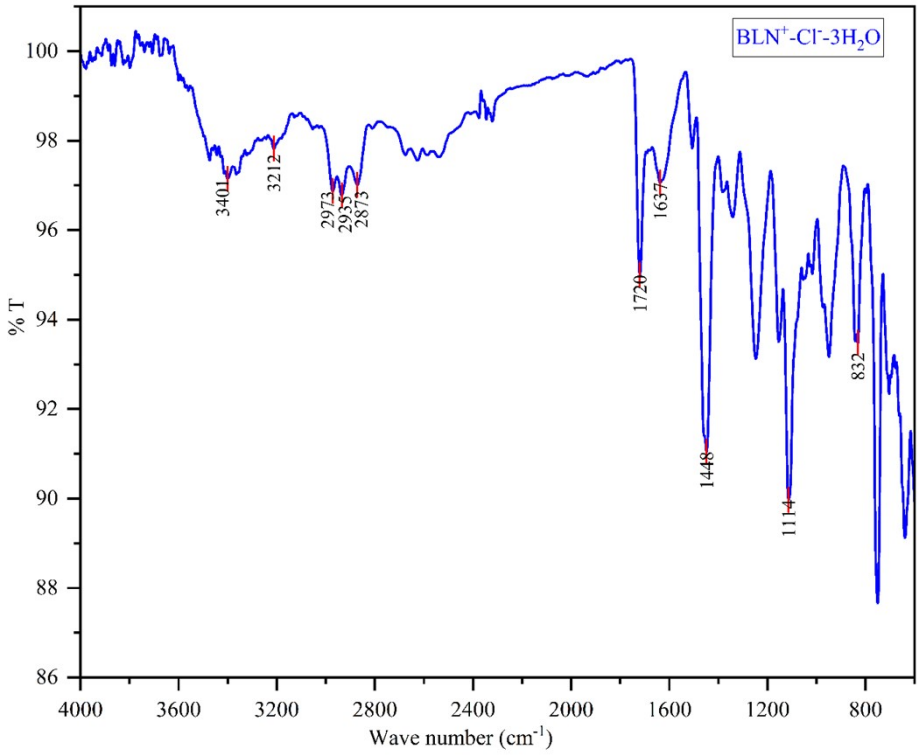

Fig. S22 FT-IR spectrum of BLN^{+}-Cl^{-}-$3H_2O$.

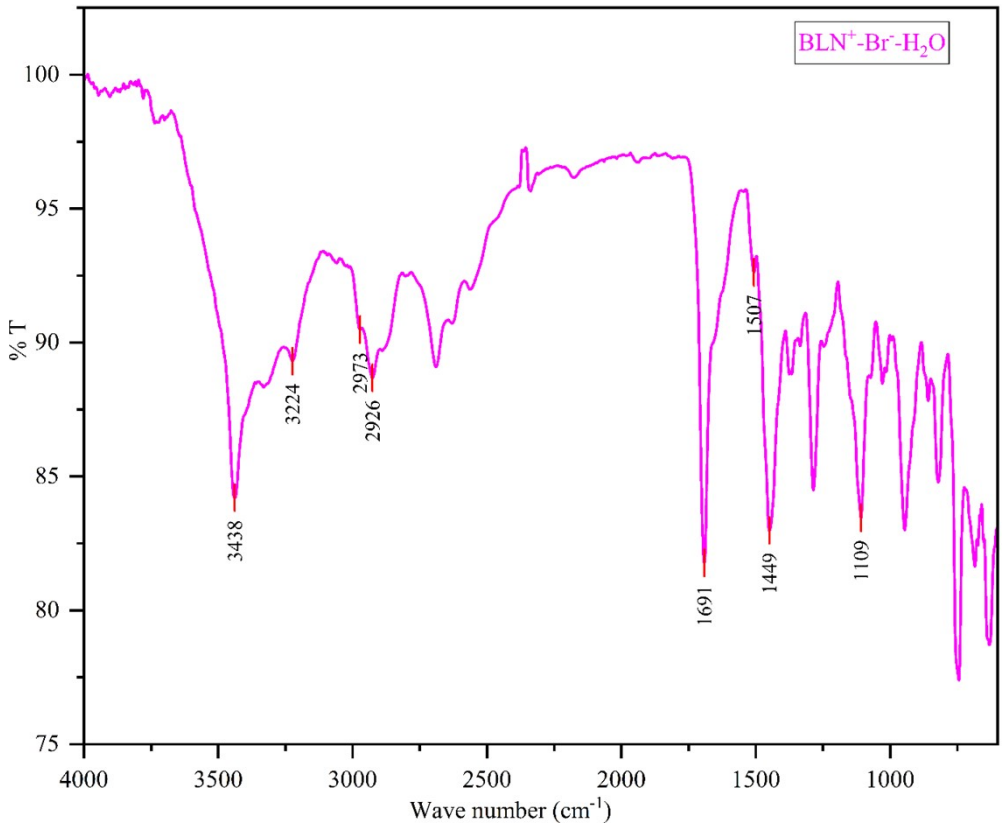

Fig. S23 FT-IR spectrum of BLN^{+}-Br^{-}-H_2O.

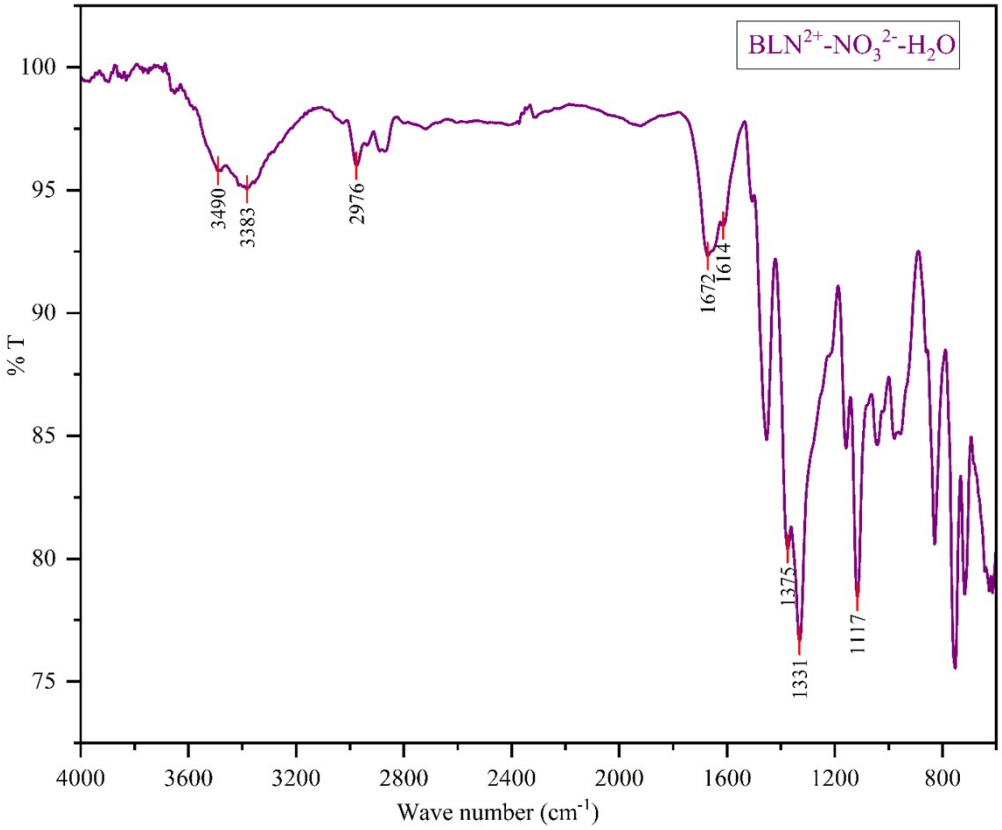

Fig. S24 FT-IR spectrum of BLN^{2+}-NO_3^{2-}-H_2O.

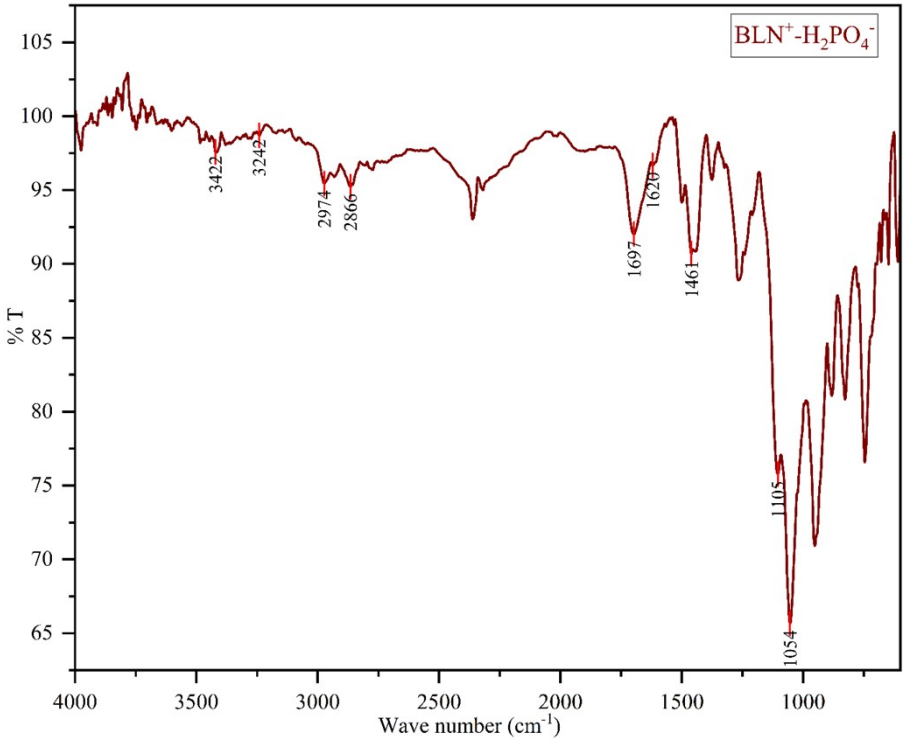

Fig. S25 FT-IR spectrum of BLN^{+}-H_2PO4^{-}.

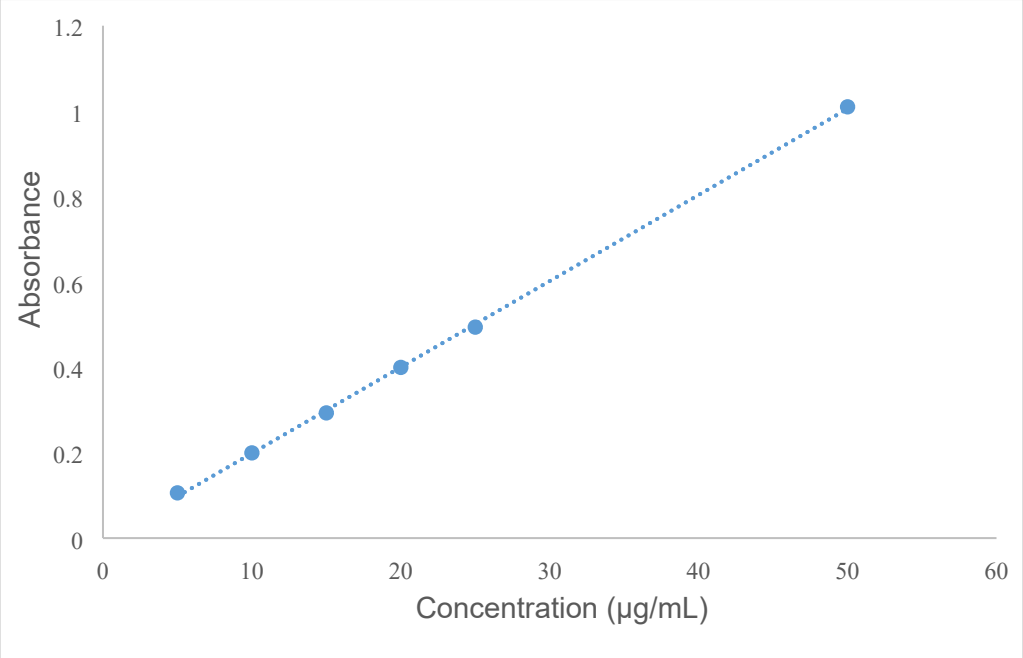

Fig. S26 BLN linearity plot in buffer pH-1.2 at 272 nm.

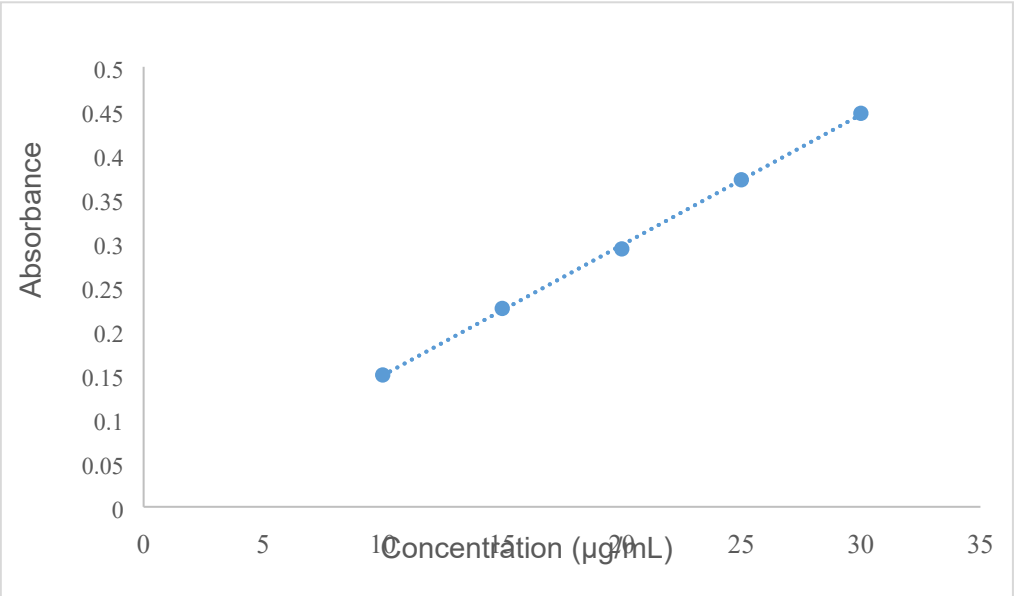

Fig. S27 BLN linearity plot in buffer pH-6.8 at 275 nm.

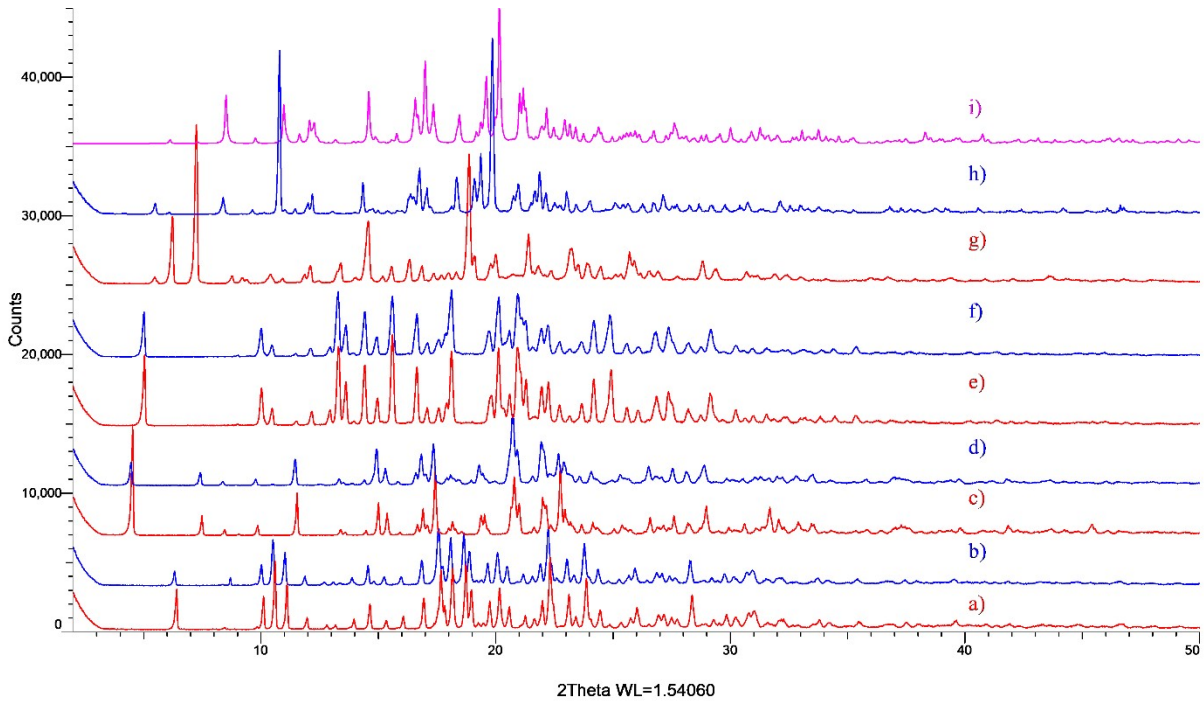

Fig. S28 PXRD overlay of solubility samples after 24 hrs a) BLN^{+}-Cl^{-}-$3H_2O$ pH-1.2 before solubility b) BLN^{+}-Cl^{-}-$3H_2O$ pH-1.2 after solubility c) BLN^{+}-Br^{-}-H_2O pH-1.2 before solubility d) BLN^{+}-Br^{-}-H_2O pH-1.2 after solubility e) BLN^{2+}-NO_3^{2-}-H_2O pH-1.2 before solubility f) BLN^{2+}-NO_3^{2-}-H_2O pH-1.2 after solubility g) BLN^{+}-H_2PO_4 pH-1.2 before solubility h) BLN^{+}-$H_2PO_4^{-}$ pH-1.2 after solubility i) BLN^{+}-H_2PO_4-Cl^{-}-$3H_2O$ experimental.

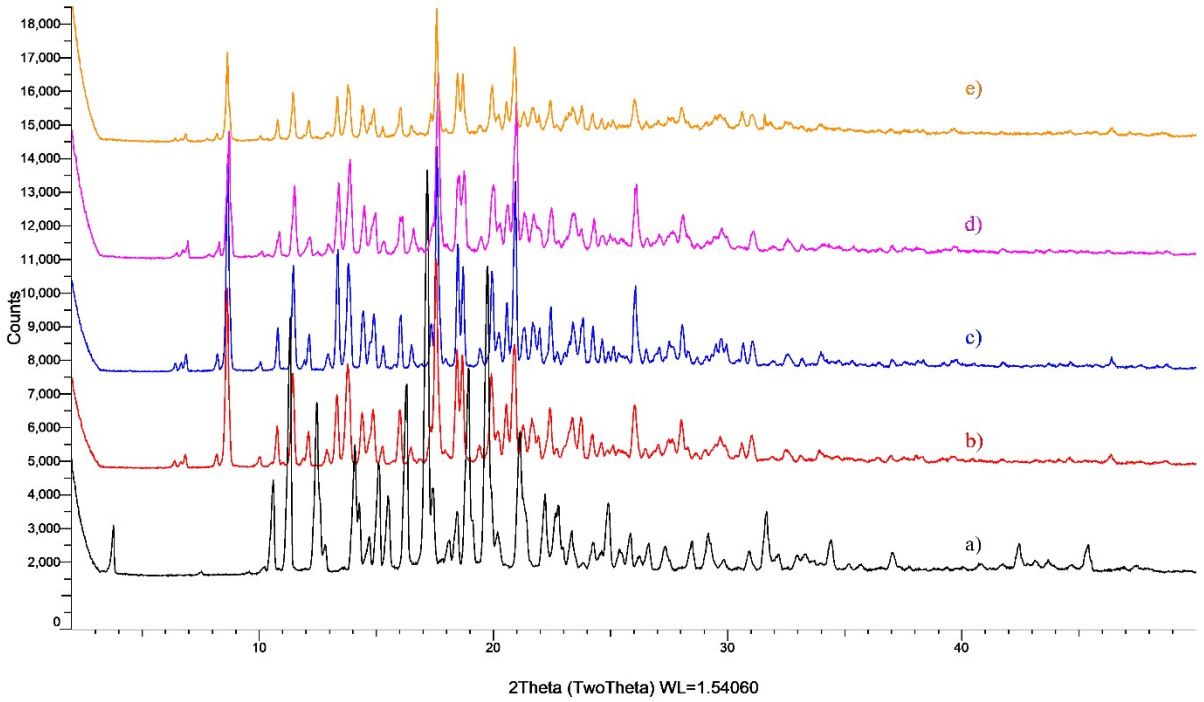

Fig. S29 PXRD overlay of solubility samples after 24 hrs a) BLN Form-I b) BLN^{+}-Cl^{-}-$3H_2O$ pH 6.8 after solubility c) BLN^{+}-Br^{-}-H_2O pH-6.8 after solubility d) BLN^{2+}-NO_3^{2-}-H_2O pH-6.8 after solubility e) BLN^{+}-$H_2PO_4^{-}$ pH-6.8 after solubility.

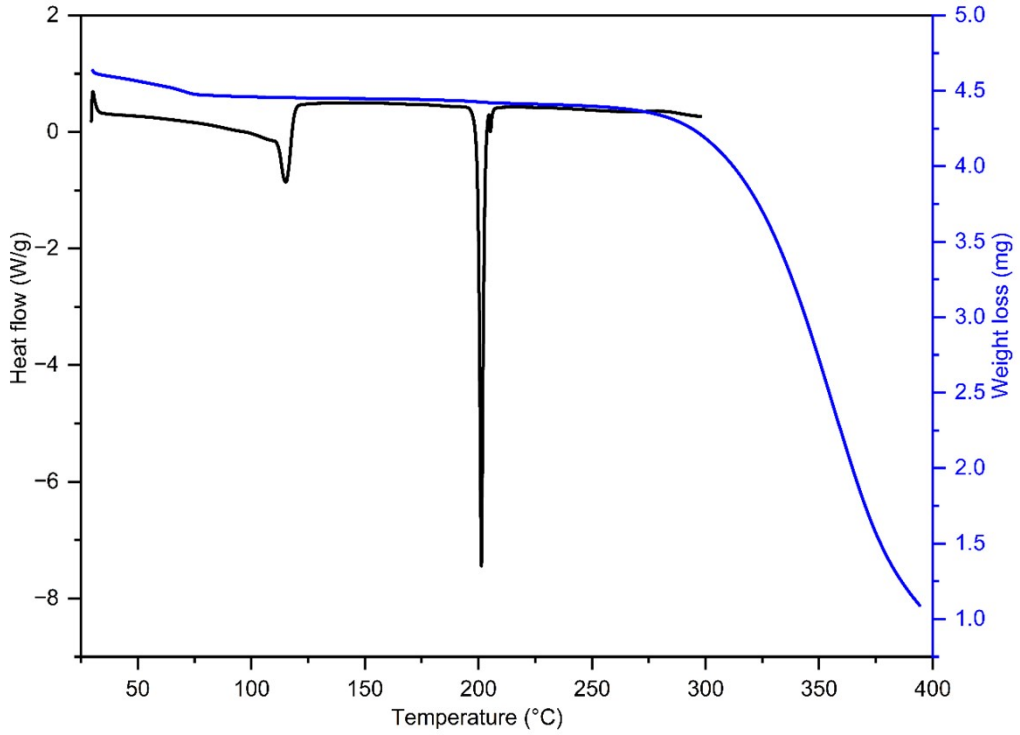

Fig. S30 DSC-TGA plot of BLN^{+}-Br^{-}-H_2O after pH-6.8 solubility.

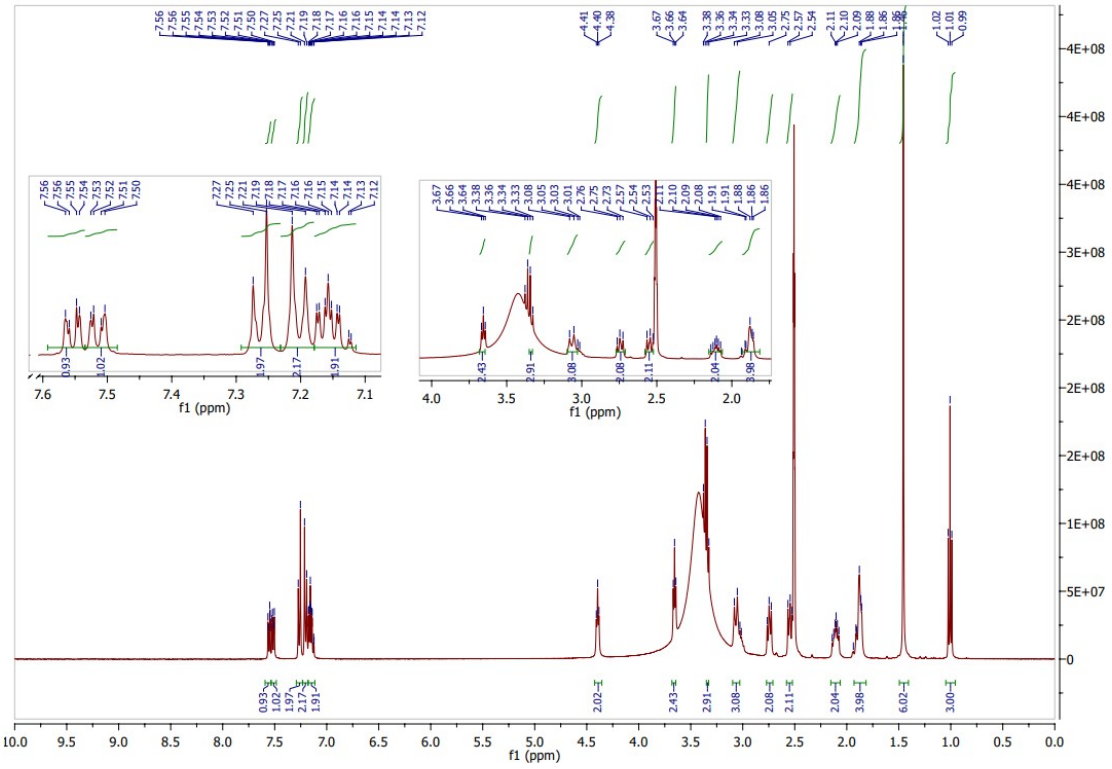

Fig. S31 ^{1}H NMR spectrum of BLN^{+}-Br^{-}-H_2O pH-6.8 after solubility.